Sparse representation-based ECG signal enhancement and QRS detection

2016 Physiol. Meas. 37 2093

(http://iopscience.iop.org/0967-3334/37/12/2093)

IOP Publishing | Institute of Physics and Engineering in Medicine Physiological Measurement

Physiol. Meas. **37** (2016) 2093–2110 doi:10.1088/0967-3334/37/12/2093

Sparse representation-based ECG signal enhancement and QRS detection

Yichao Zhou[1,2], Xiyuan Hu[2,4], Zhenmin Tang[1] and Andrew C Ahn[3]

[1] School of Computer Science, Nanjing University of Science and Technology, Nanjing 210094, People's Republic of China
[2] High Technology Innovation Center (HITIC), Institute of Automation, Chinese Academy of Sciences, Beijing 100190, People's Republic of China
[3] Beth Israel Deaconess Medical Center & Massachusetts General Hospital, Harvard Medical School, Boston, MA 02215, USA

E-mail: wingegg_313@126.com, xiyuan.hu@ia.ac.cn and aahn1@mgh.harvard.edu

Received 21 May 2016, revised 28 September 2016
Accepted for publication 6 October 2016
Published 4 November 2016

Abstract

Electrocardiogram (ECG) signal enhancement and QRS complex detection is a critical preprocessing step for further heart disease analysis and diagnosis. In this paper, we propose a sparse representation-based ECG signal enhancement and QRS complex detection algorithm. Unlike traditional Fourier or wavelet transform-based methods, which use fixed bases, the proposed algorithm models the ECG signal as the superposition of a few inner structures plus additive random noise, where these structures (referred to here as atoms) can be learned from the input signal or a training set. Using these atoms and their properties, we can accurately approximate the original ECG signal and remove the noise and other artifacts such as baseline wandering. Additionally, some of the atoms with larger kurtosis values can be modified and used as an indication function to detect and locate the QRS complexes in the enhanced ECG signals. To demonstrate the robustness and efficacy of the proposed algorithm, we compare it with several state-of-the-art ECG enhancement and QRS detection algorithms using both simulated and real-life ECG recordings.

Keywords: ECG enhancement, QRS complex detection, sparse representation, dictionary learning

(Some figures may appear in colour only in the online journal)

[4] Author to whom all correspondence should be addressed.

1. Introduction

The electrocardiogram (ECG) is a recording of electrical cardiac activity and is commonly used to evaluate the health of the human heart. As portable devices and electronic medical records have increased the acquisition of ambulatory ECG measures, ECG recordings—which are increasingly longer in duration—are inevitably contaminated by noises and artifacts including additive random noise, baseline wandering (BW) caused by motion and muscle artifact along with ambient electrical fields. Therefore, enhancement of the ECG signal, usually as a preprocessing step, will not only ease the clinical evaluation of ECG waveforms but will also assist in improving the overall accuracy of automatic QRS complex detection (Pal and Mitra 2012, Ning and Selesnick 2013, Akhbari *et al* 2016). Additionally, the accuracy of the beat-to-beat (RR) intervals extracted from ECG recordings is crucial for reliable heart rate variability (HRV) analysis.

For ECG signal denoising and baseline correction, traditional filtering-based approaches were initially used to remove these signal contaminations based on their frequency responses (Addison 2005). Although these types of algorithms can suppress high-frequency noise, they may also distort the spike waveforms in the ECG signals because these spike waveforms, like the QRS complex, usually have a very wide frequency spectrum. To overcome the drawbacks of the filtering-based approaches, some recent advances in adaptive signal processing techniques have been introduced (Blanco-Velasco *et al* 2008, Kabir and Shahnaz 2012, Tracey and Miller 2012, Yi *et al* 2013, Abdelmounim *et al* 2014, Zhou *et al* 2015). For example, because the spike waves found in ECG signals are similar to some wavelet bases, Abdelmounim *et al* proposed a wavelet-based thresholding algorithm that used wavelet transforms to characterize and locate these waves and subsequently used thresholding techniques to remove the noise (Abdelmounim *et al* 2014). Because wavelet transform cannot remove smoothly-varying baseline wandering effectively, the authors used a very narrow low-pass filter to remove the baseline wandering after the denoising process. In addition to the fixed basis projection algorithms, such as Fourier and Wavelet transform-based algorithms, empirical mode decomposition (EMD) has also been introduced to ECG signal processing. When the ECG signal is decomposed by EMD, the high-frequency noise, the ECG waveforms and the baseline will each be variably distributed to different intrinsic mode functions (IMFs). Using this feature, Blanco-Velasco *et al* proposed a novel EMD-based algorithm that can remove both the high-frequency noise and the baseline wandering with only small signal distortion (Blanco-Velasco *et al* 2008). Also, Pal and Mitra applied EMD to remove both baseline wandering and noise from ECG signals, and furthermore, improved QRS detection using the features of the IMFs (Pal and Mitra 2012). However, because of the mode-mixing phenomenon (Hu *et al* 2012) in the EMD, most QRS complexes cannot be fully confined to a single IMF; they are usually spread to multiple IMFs and mixed with the noise in the first few IMFs. By combining the advantages of EMD and wavelet transforms, Kabir and Shahnaz proposed an EMD-wavelet domain-based ECG denoising algorithm (Kabir and Shahnaz 2012) that uses wavelets to improve the denoising results in these first few IMFs.

After ECG signal preprocessing is complete, the next step is automatic QRS complex detection, which has been studied for more than 30 years. Because of the unique wave pattern of the QRS complex, the template matching-based algorithm was first introduced to detect the QRS complex by calculating the correlation between the template and the detected signals (Dobbs *et al* 1984, Chan *et al* 2006). This type of approach, however, is as heavily dependent on prior knowledge as it is on the selection of suitable templates. Therefore, some signal features, e.g. the slope of the R-wave, have been used rather than the template waves to detect and locate the QRS complex. These algorithms generally need to compute the derivatives of the ECG

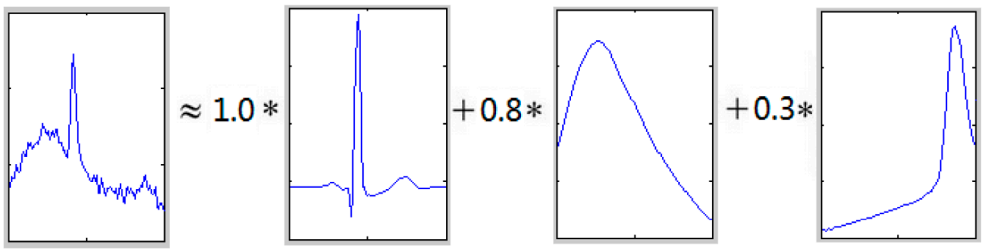

Figure 1. Example of sparse representation of a segment of an ECG recording.

signals (Arzeno *et al* 2008, Ning and Selesnick 2013). Because high-frequency noise will also be amplified by these derivatives, their accuracy and sensitivity will be reliant on the denoising results from the pre-processing steps. As many recent signal decomposition algorithms, e.g. EMD, wavelet-based algorithms, and time-frequency analysis (TFA), have been applied to ECG signal enhancement, these previously proposed QRS detection algorithms can also be applied to the extracted intrinsic mode function (Pal and Mitra 2012), the wavelet coefficients (Zidelmal *et al* 2012, Bouaziz *et al* 2014) or the Shannon energy in TFA (Zhu and Dong 2013, Zidelmal *et al* 2014) to improve the QRS detection accuracy. However, the main drawback of this type of approach is its sensitivity to the selection of suitable subcomponents or wavelet basis functions, which in turn affects the QRS detection efficiency. Recently, some machine learning-based approaches, e.g. artificial neural network (ANN), have also been applied to the field of QRS complex detection (Arbateni and Bennia 2014). Besides the QRS detection algorithm that only use ECG signals, some heart beat detection algorithms that adopt multimodal measurement have also been introduced (Johnson *et al* 2015).

Although the QRS complex vary in morphology due to different lead placements and inter-individual variability, it possesses repetitive (not periodic) patterns that are still quite distinct from random noise and baseline wandering. Therefore, if these patterns can be learned adaptively from a given ECG recording, the QRS complex can be represented by these learned patterns (which we call inner structures) with great efficiency and effectiveness. To address this task, the signal's sparse and redundant representation model (Aharon *et al* 2006, Tosic and Frossard 2011) comes to mind. In this model, a redundant dictionary is trained using either the input signal or a training set, and the signal to be analyzed can then be sparsely approximated using the atoms in the trained dictionary. For example, as shown in figure 1, when given a segment of an ECG recording, we assume that this segment can be approximated using a linear combination of only few atoms in a well-trained dictionary. The residual component of this segment can then be viewed as additive random noise.

Because the atoms in the dictionary are trained from the actual ECG recordings of interest, they can depict the inner structures of these specific ECG recordings. If we further analyze the atoms in the dictionary using certain statistical measures, we can then select suitable atoms, use them to reconstruct clean ECG signals, and remove both noise and baseline wandering. Furthermore, we can modify these selected atoms by only retaining the peak point of each, and these modified atoms can then be viewed as impulse functions and can be used to locate the QRS complex. Therefore, our proposed sparse representation-based ECG enhancement and QRS detection algorithm consists of three steps: (1) training of a redundant dictionary using the input ECG recording; (2) separation of the atoms in the dictionary into two parts based on their kurtosis, followed by reconstruction of the clean ECG signal using those atoms with high kurtosis values; and (3) modification of those selected atoms before using them to locate

the QRS complex. Experimental comparisons are used to evaluate the performance of our proposed algorithm for ECG signal enhancement and QRS detection under noisy conditions.

The remainder of this paper is organized as follows. In section 2, we review the fast sparse representation algorithm. In section 3, we present our ECG signal denoising and baseline correction algorithm, and in section 4, our QRS complex detection algorithm is proposed. Then, we perform experiments using simulated and real-life ECG signals and discuss the results in section 5. Finally, section 6 contains our concluding remarks.

2. Sparse representation of signals

Given an input signal $\boldsymbol{y} \in \mathbb{R}^n$, the sparse representation model assumes that this signal can be approximated as $\boldsymbol{y} \approx \boldsymbol{D}\boldsymbol{\alpha}$, where $\boldsymbol{D} \in \mathbb{R}^{n \times m}$ is a dictionary matrix and $\boldsymbol{\alpha} \in \mathbb{R}^m$ gives the representation coefficients. Because each column of the dictionary matrix $\boldsymbol{D}$ is called an atom, the approximation of the input signal can be viewed as a weighted summation of these atoms and their weights (as given by the coefficients in $\boldsymbol{\alpha}$). Usually, the dictionary $\boldsymbol{D}$ is assumed to be redundant, which means that the number of atoms in the dictionary should be much greater than the length of the input signals; and the coefficients $\boldsymbol{\alpha}$ are assumed to be sparse, which means there are only few non-zero weights (coefficients) in $\boldsymbol{\alpha}$, i.e. $\|\boldsymbol{\alpha}\|_0$ is very small. This then implies that the input signal $\boldsymbol{y}$ can be approximated using only few atoms (with corresponding weights that are not equal to zero) from the dictionary matrix $\boldsymbol{D}$. Therefore, these atoms can be viewed as a description of the inner structures of the input signal.

The most important step to enable application of this model to practical real-life signals is to learn a dictionary that is suitable for a family of signals. Given a set of example signals, $\boldsymbol{Y} = \{\boldsymbol{y}_i\}_{i=1}^N$, dictionary learning algorithms try to train a dictionary $\boldsymbol{D}$ that can sparsify and minimize the approximation error of these signals. This problem can be formulated as

$$\hat{\boldsymbol{D}} = \arg \min_{\boldsymbol{D}, \boldsymbol{\alpha}_i} \sum_{i=1}^{N} \|\boldsymbol{y}_i - \boldsymbol{D}\boldsymbol{\alpha}_i\|_2^2, \text{ s.t. } \forall i, \|\boldsymbol{\alpha}_i\|_0 < k, \tag{1}$$

where k is the parameter that constrains the maximum number of atoms that can be used to approximate the signal. The optimization problem above is very complex, because both the dictionary and the representation coefficients need to be estimated. Most existing approaches to solving this problem, like MOD and K-SVD algorithm, etc, consist of two steps (Aharon *et al* 2006, Engan *et al* 2007, Tosic and Frossard 2011): (1) given an estimated dictionary, compute sparse representation coefficients $\boldsymbol{\alpha}_i$; and (2) using the known representation, update dictionary $\boldsymbol{D}$. This approach will provide an approximate solution but can be highly time-consuming because of the slow convergence rate that results from this alternative optimization style.

To accelerate the solving procedure for the problem presented in equation (1), Smith and Elad proposed an improved dictionary learning algorithm that uses multiple dictionary updates and coefficient reuse techniques (Smith and Elad 2013). They then formulated the optimization task as

$$\{\hat{\boldsymbol{D}}, \hat{\boldsymbol{A}}\} = \arg \min_{\boldsymbol{D}, \boldsymbol{A}} \|\boldsymbol{Y} - \boldsymbol{D}\boldsymbol{A}\|_F^2, \text{ s.t. } \boldsymbol{A} \odot \boldsymbol{M} = 0, \tag{2}$$

where $\boldsymbol{A} = [\boldsymbol{\alpha}_1, \boldsymbol{\alpha}_2, \cdots, \boldsymbol{\alpha}_N]$; $\odot$ denotes the entry-wise (Schur) multiplication of two equally-sized matrices; and $\boldsymbol{M}$ is a mask matrix of zeros and ones with $M(i, j) = 1$ if $A(i, j) = 0$, and zeros elsewhere. The requirement $\boldsymbol{A} \odot \boldsymbol{M} = 0$ then forces all zero entries in A to remain intact

(Smith and Elad 2013). This constraint optimization problem can also be solved using a block-coordinate-descent approach, i.e. for a fixed $\boldsymbol{A}$, $\boldsymbol{D}$ can be updated using

$$\hat{\boldsymbol{D}} = \arg\min_{\boldsymbol{D}} \|\boldsymbol{Y} - \boldsymbol{D}\boldsymbol{A}\|_F^2 = \boldsymbol{Y}\boldsymbol{A}^T(\boldsymbol{A}\boldsymbol{A}^T)^{-1} = \boldsymbol{Y}\boldsymbol{A}^{\dagger}, \tag{3}$$

and is then followed by an update of each column in $\boldsymbol{A}$ by fixing $\boldsymbol{D}$ and solving

$$\hat{\boldsymbol{\alpha}_i} = \arg\min_{\boldsymbol{\alpha}_i} \|\boldsymbol{y}_i - \boldsymbol{D}_i\boldsymbol{\alpha}_i\|_2^2 = \boldsymbol{D}_i^{\dagger}\boldsymbol{y}_i, \tag{4}$$

where $\boldsymbol{D}_i$ is a sub-matrix of $\boldsymbol{D}$ that contains only the atoms that support this representation. When the complete representation $\boldsymbol{A}$ is derived, the mask matrix $\boldsymbol{M}$ will then be updated based on $\boldsymbol{A}$. While this alternative iteration style is similar to the styles used in both MOD and K-SVD, it is much faster because of the use of the constraint mask matrix $\boldsymbol{M}$. More detailed discussions and implementations of this improved dictionary learning algorithm can be found in the (Smith and Elad 2013).

3. ECG signal denoising and baseline correction

In this section, we discuss the sparse representation-based ECG signal enhancement algorithm, including the ECG signal denoising and baseline correction aspects. Because typical ECG signals contain the P-wave, the QRS complex and the T-wave, they can be represented sparsely by the inner structures (or atoms). However, to the best of the authors' knowledge, there are no dictionaries or bases that are fully depictive or representative of random noise. While smoothly-varying baseline wandering can also be represented using some harmonic atoms, similar to DCT-bases, their kurtoses are always much smaller than the kurtosis of typical ECG waves. Consequently, our ECG signal enhancement algorithm comprises three steps: (1) using the given ECG signals to generate a training set and then learning a suitable dictionary that fits this signal; (2) using the trained dictionary to derive a sparse representation of the ECG signal provided; and (3) computation of the kurtosis of each atom in the dictionary and reconstructing the clean ECG signal using the atoms with large kurtosis values.

3.1. Dictionary training of ECG signals

Because our algorithm is based on the sparse and redundant representation of the signal, the input signals will be processed using an overlapped segment-by-segment style. This means that for an input signal $s(t)$ of length L, if we define the length of a segment to be l, then $s(t)$ will be divided into multiple segments as $s_i(t) = [s(i), s(i+1), \cdots, s(i+l-1)]$ with $i = 1, \tau+1, 2\tau+1, \cdots, L-l+1$, where $\tau < l$ denotes the time shift; then, each segment $s_i(t)$ will be processed or reconstructed successively as $\hat{s}_i(t)$. Then, the processed or reconstructed signal $\hat{s}(t)$ can be calculated using a weighted average of all the processed segments as

$$\hat{s}(t) = \frac{1}{n+1}\sum_{k=0}^{n} \hat{s}_{i+k\tau}(t - i - k\tau), \text{ with } i < t < i + n\tau. \tag{5}$$

Thus, if the segment length is chosen to be l, the size of dictionary $\boldsymbol{D}$ should be $l \times m$ with $m \gg l$; and the number of segments contained in the training set should be much larger than m.

Theoretically, we can randomly select sufficient segments from a standard ECG signal database as a universal training set and then learn a universal dictionary for processing of all input ECG signals across patients. However, ECG recordings often contain a significant amount of diversity, which stems from differing lead placements, inter-individual variabilities

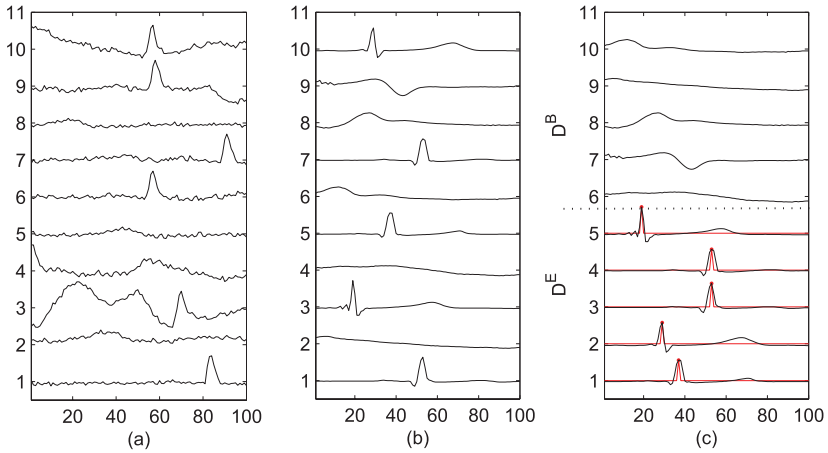

Figure 2. Examples of training set and learned dictionary: (a) examples of raw signal segments used in the training set; (b) some atoms selected from the dictionary that were learned from the training set; (c) selected atoms from the separate sub-dictionaries (denoted by $\boldsymbol{D}^B$ and $\boldsymbol{D}^E$). Noted that the atoms labeled in (b) correspond to the atoms labeled in (c).

and conduction pathologies. This indicates that, given a specific ECG signal, this over-generalized dictionary may not achieve the best representation (or approximation) capacity for those specific waveforms of interest. Therefore, in this paper, we use an individual ECG signal to construct the training set and then learn a dictionary that fits for itself using an improved dictionary learning algorithm (Smith and Elad 2013) described in section 2. In this way, the learned dictionary is both parsimonious to the individual ECG and efficient in sparsely representing the data. Moreover, due to the improved dictionary algorithm, the time required for the training process has been greatly reduced, and an individual, case-by-case learning approach becomes computationally and practically feasible. Therefore, in this paper, we will train a dictionary for a given ECG signal by using its own waveform as a reference.

Although ECG signals that are recorded from different people may have different wave patterns, the wave patterns within an individual ECG lead are repetitive, and a specific waveform can be highly representative of the waveforms seen in the whole time-series of that particular lead. Furthermore, partitioned segments can be randomly selected from a long-term ECG recording to train the dictionary efficiently, rather than use the entire signal. For our proposed dictionary training process based on a given ECG signal (as shown in figure 4(a)), we randomly select segments containing 50 times the number of atoms in the dictionary to construct our training set. Some of the segment examples are shown in figure 2(a). We subsequently use the improved dictionary learning algorithm[5] to train a dictionary using this training set. Figure 2(b) shows some of the atoms in the trained dictionary from this ECG recording, from which we see that some of these atoms reveal distinguishing ECG signal features. Of note, our training algorithm does not employ a shift-invariant dictionary as proposed by Mailhé *et al* (2008). As can be seen in figure 2(b), the atoms in the dictionary may have similar waveforms but are shifted in time relative to each other. Attempts at using a time-invariant dictionary were encountered with exceedingly slow processing since the algorithm required determination of

[5] This algorithm is described briefly in section 2, and its source codes can be downloaded from www.cs.technion.ac.il/~elad/Various/ImprovedDL.rar.

not only the most suitable atoms but also the optimal shifting parameter in the reconstructing process.

3.2. Synchronous denoising and baseline correction

For a given ECG recording $s(t)$, we assume that this recording contains three component signals: a clean ECG signal $s^E(t)$, baseline wandering artifacts $s^B(t)$, and additive random noise. The ECG recording can thus be modeled as the superposition of these components in the form

$$s(t) = s^E(t) + s^B(t) + \text{noise}. \tag{6}$$

Then, using the already trained dictionary $\boldsymbol{D}$, the input signal $s(t)$ can be processed on a segment-by-segment basis. For a signal segment $\boldsymbol{s}_i = s_i(t)$, we use the orthogonal matching pursuit (OMP) algorithm (Pati *et al* 1993) to compute its sparse representation from dictionary $\boldsymbol{D}$, which is denoted by $\boldsymbol{\alpha}_i$. Because the dictionary $\boldsymbol{D}$ is trained based on this recording itself, it can effectively and sparsely represent the ECG signal and the baseline while excluding the random noise. This means that we can assume that the reconstructed segment $\hat{\boldsymbol{s}}_i$ retains most of the useful information contained in the original segment in the form

$$\hat{\boldsymbol{s}}_i = \boldsymbol{D}\boldsymbol{\alpha}_i \approx \boldsymbol{s}_i^E + \boldsymbol{s}_i^B. \tag{7}$$

Additionally, because the ECG signals usually have sharp peaks and smoothly-varying baselines, this significant difference should also be reflected in the learned dictionary (as shown in figure 2(b)). Therefore, we compute the kurtosis of each atom $\boldsymbol{d}_j$ in the dictionary $\boldsymbol{D}$ as

$$\kappa(\boldsymbol{d}_j) = \frac{E(\boldsymbol{d}_j - \mu)^4}{\sigma^4} = \frac{\frac{1}{N}\sum_{i=1}^{N}(d_j(i) - \bar{\boldsymbol{d}}_j)^4}{\left(\frac{1}{N}\sum_{i=1}^{N}(d_j(i) - \bar{\boldsymbol{d}}_j)^2\right)^2}, \tag{8}$$

where N denotes the length of $\boldsymbol{d}_j$. For smooth varying signals (like baseline wandering), most values do not deviate far from the mean value of the signal. As a consequence, according to equation (8), their kurtosis are nearly uniformly small. On the other hand, for shock signals (like the QRS complex), although most values lie close to the mean, there are few data points with very large bias values. This yields a large fourth central moment (numerator) and a relatively small standard deviation (denominator) which collectively lead to large kurtosis values. Figure 3 shows a statistical histogram of $\kappa(\boldsymbol{d}_j)$ of a dictionary $\boldsymbol{D}$. Then, given a threshold parameter λ, the atoms in $\boldsymbol{D}$ can be clearly divided into two sub-dictionaries, denoted by $\boldsymbol{D}^E$ and $\boldsymbol{D}^B$, with $\boldsymbol{D}^E = \{\boldsymbol{d}_j; \kappa(\boldsymbol{d}_j) > \lambda\}$ and $\boldsymbol{D}^B = \{\boldsymbol{d}_j; \kappa(\boldsymbol{d}_j) \leqslant \lambda\}$. The sub-dictionary $\boldsymbol{D}^E$ contains the atoms that have sharp peaks and large kurtosis values; in contrast, the sub-dictionary $\boldsymbol{D}^B$ includes smoothly-varying atoms that have small kurtosis values. Some of the atoms from these two separate sub-dictionaries can be found in figure 2(c). Also, if we use $\boldsymbol{\alpha}_i^E$ to denote the coefficients in $\boldsymbol{\alpha}$ that correspond to the atoms in the sub-dictionary $\boldsymbol{D}^E$, the clean estimated ECG signal $\hat{s}^E(t)$ can be derived based on the weighted average of all these ECG segments $\hat{\boldsymbol{s}}_i^E = \boldsymbol{D}^E\boldsymbol{\alpha}_i^E$. The overall ECG signal denoising and baseline correction algorithm can thus be summarized as shown in algorithm 1. Also, given an input ECG signal (as shown in figure 4(a)), the resulting enhanced ECG signal and the removed baseline that is derived using this algorithm can be found in figure 4(b), and are represented by the black and red lines, respectively.

Algorithm 1. ECG enhancement algorithm.

1: Input ECG recording $\boldsymbol{s}$, choose the length l for each segment, the number of atoms in the dictionary n, and a threshold λ.
2: Randomly select $50n$ of segments from $\boldsymbol{s}$ to build the training set;
3: Learn the redundant dictionary $\boldsymbol{D} \in \mathbb{R}^{l \times m}$ from the training set;
4: Compute the kurtosis of each atom $\boldsymbol{d}_j \in \boldsymbol{D}$, which is denoted as $\kappa(\boldsymbol{d}_j)$;
5: Divide the dictionary into two sub-dictionaries with $\boldsymbol{D}^E = \{\boldsymbol{d}_j; \kappa(\boldsymbol{d}_j) > \lambda\}$ and $\boldsymbol{D}^B = \{\boldsymbol{d}_j; \kappa(\boldsymbol{d}_j) \leqslant \lambda\}$;
6: **for** each segment $\boldsymbol{s}_i$ in $\boldsymbol{s}$ **do**
7: Compute its sparse representation coefficient $\boldsymbol{\alpha}_i$ using dictionary $\boldsymbol{D}$;
8: Only retain the coefficients related to the sub-dictionary $\boldsymbol{D}^E$ as $\boldsymbol{\alpha}_i^E$;
9: Reconstruct the clean ECG segment as $\hat{\boldsymbol{s}}_i^E = \boldsymbol{D}^E \boldsymbol{\alpha}_i^E$;
10: **end for**
11: **return** Reconstruct the clean ECG signal $\hat{s}^E(t)$ using the weighted average of all segments $\hat{\boldsymbol{s}}_i^E$;

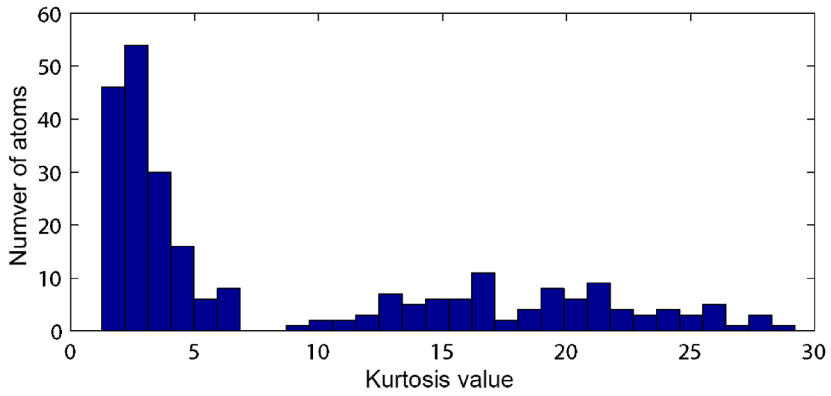

Figure 3. Statistical histogram of the kurtosis of all atoms in learned dictionary $\boldsymbol{D}$.

3.2.1. Some implementation details. In algorithm 1, the length l of each signal segment depends on the sampling rate of the ECG recording. If the sampling rate is PHz, we set the signal segment length to be $0.8P$ samples in all of our experiments. We set the number of atoms in the dictionary to be $2P$ because it should be greater than the segment length to ensure that the learned dictionary is redundant. After the length l has been decided, the parameter τ in equation (5) can be determined. In practice, a smaller τ generates better results but has the undesired side-effect of increased algorithm's computational time. In all experiments in this paper, we designated $\tau = 0.05l$. The other parameter that must be considered is the maximum number of atoms used for signal reconstruction, which reflects the sparseness of the representation. Based on our own preliminary tests, this approach is quite robust for reconstruction of noisy ECG signals. For this reason, we set the maximum number of atoms to be $0.1P$. The last parameter to be considered is the threshold λ. In most cases, it can be estimated from the statistical histogram as shown in figure 3. However, there still remains the risk that the training process fails to converge towards a satisfactory dictionary, and in such cases, the estimation of λ may be incorrect. As a result, in all the experiments discussed later in this paper, λ was empirically chosen to be a value of 6 based on prior experimentations (figure 3 is a case example) and on the recognition that kurtosis of standard Gaussian distribution is 3 and that shock signals are nearly always much sharper than Gaussian function.

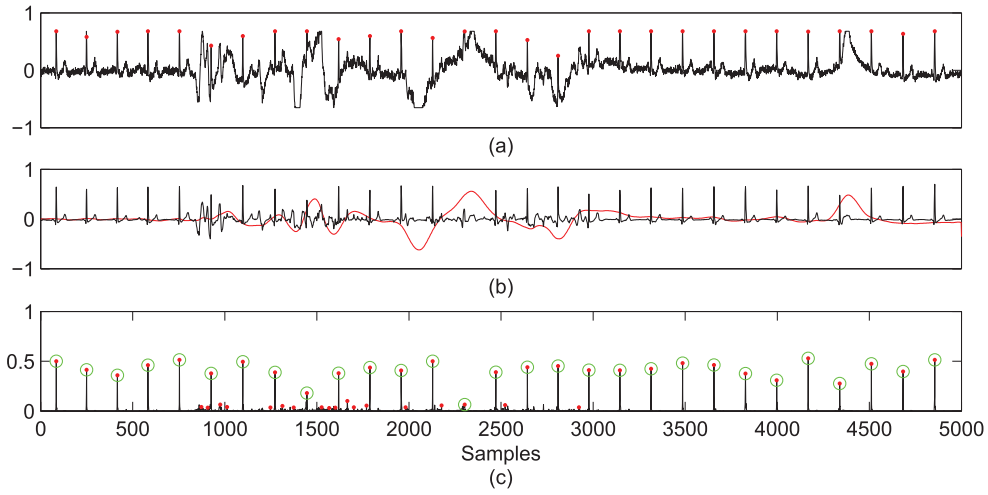

Figure 4. ECG enhancement and QRS complex detection. (a) ECG recording s00377 from PhysioNet MIMIC II waveform database matched subset; (b) denoised ECG signal and removed baseline; (c) reconstructed QRS peak information signal, local maxima points (denoted by red dots) and detected QRS complex locations (denoted by green circles).

4. QRS complex detection

Because the QRS complex is generated by ventricular depolarization, it consists in most ECG signals of a very sharp peak R-wave and two other waves with smaller amplitudes, called the Q-wave and the S-wave. As shown in section 3, the distinctive features of the QRS complex can be characterized effectively using the atoms in the sub-dictionary $\boldsymbol{D}^E$. Therefore, these atoms can not only be used to reconstruct a clean ECG signal but can also locate the QRS complex with some modifications. The steps required to detect the QRS complex using these atoms are described below.

First, for each atom $\boldsymbol{d}_j$ in the sub-dictionary $\boldsymbol{D}^E$, we only retain the point with the largest absolute value in $\boldsymbol{d}_j$ and set all other points to zero. That is, if we denote the modified atom of $\boldsymbol{d}_j$ as $\tilde{\boldsymbol{d}}_j$, we have

$$\tilde{d}_j(i) = \begin{cases} |d_j(i)|, & \text{if } |d_j(i)| = \max(|\boldsymbol{d}_j|) \\ 0, & \text{otherwise } i = 1, 2, \cdots, l \end{cases} \tag{9}$$

Here, we use the maximum of the absolute value rather than the maximum value because the QRS at different lead placements will not always have a positive value. Some examples of this modification can be seen in sub-dictionary $\boldsymbol{D}^E$ in figure 2(c), where the black and red lines denote the original trained atoms $\boldsymbol{d}$ and the modified atoms $\tilde{\boldsymbol{d}}$, respectively.

We also use these modified atoms $\tilde{\boldsymbol{d}}_j$ and their corresponding coefficients $\boldsymbol{\alpha}^E$ to reconstruct the QRS peak information signal $\tilde{\boldsymbol{s}}^{pk}$, as shown in figure 4(c). (Figure 4(b) shows the enhanced ECG signal that was derived using the original atoms $\boldsymbol{d}_j$ and their coefficients $\boldsymbol{\alpha}^E$.) Then, we detect all the local extremum points in this information signal $\tilde{\boldsymbol{s}}^{pk}$ with values that are larger than a small threshold $\eta = 0.05 \max(|\tilde{\boldsymbol{s}}^{pk}|)$ and mark these points as the QRS candidate locations, as indicated by the red dots in figure 4(c).

Although most of the noise and the baseline wandering can be removed in the pre-processing step, a little noise may still remain in the enhanced ECG signal. The remaining noise will also lead to local extremum points and will thus be detected. Therefore, as a final step, we use a sliding window to remove those extrema that were derived from noise. In the window, we compute the absolute values of all extrema. If the value of the largest extremum is three times larger than the value of the second largest extremum, then the largest extremum will be preserved; otherwise, all extrema in the window are removed from the candidate set. As shown in figure 4(c), the green circles represent the final detected QRS complex, and their locations in the original input signal are marked using red dots in figure 4(a). The complete QRS complex detection algorithm is summarized as shown in algorithm 2.

5. Experimental results and discussion

In this section, we evaluate the performance of our proposed algorithm in terms of the following two aspects: (1) ECG signal enhancement, and (2) QRS complex detection.

5.1. ECG enhancement experiments

For the ECG signal denoising and baseline correction aspect, figure 4 shows an example of a real-life ECG recording enhancement that was derived using our algorithm 1. Because the original ECG recording contains several hours of data, we only show 5000 samples (approximately 39 s) of this signal in figure 4(a). The denoised and baseline corrected ECG signal and the removed baseline are shown in figure 4(b) as black and red lines, respectively. From this, we see that the baseline has clearly been removed from the original input ECG signal.

Algorithm 2. QRS complex detection algorithm.

1: Input the trained sub-dictionary $\boldsymbol{D}^E$ and the coefficients of each segment as $\boldsymbol{\alpha}_i^E$ derived from algorithm 1;
2: Modify all atoms in $\boldsymbol{D}^E$ using equation (9) and derive the modified sub-dictionary $\tilde{\boldsymbol{D}}^E$;
3: **for** each segment $\boldsymbol{s}_i$ **do**
4: Compute the QRS peak information segment as $\tilde{\boldsymbol{s}}_i^{pk} = \tilde{\boldsymbol{D}}^E \boldsymbol{\alpha}_i^E$;
5: **end for**
6: Reconstruct the QRS peak information signal $\tilde{\boldsymbol{s}}^{pk}$ using the weighted average of all segments $\tilde{\boldsymbol{s}}_i^{pk}$;
7: Detect all local extremum points with absolute value larger than $0.05 \max(|\tilde{\boldsymbol{s}}^{pk}|)$;
8: **for** each local extremum location j **do**
9: Select a neighborhood window $\tilde{\boldsymbol{s}}_j^{pk} = [\tilde{s}^{pk}(j-\Delta),\ \tilde{s}^{pk}(j+\Delta)]$;
10: Compute the largest and second largest values of $|\tilde{\boldsymbol{s}}_j^{pk}|$ as m_1 and m_2, respectively;
11: **if** $\tilde{s}^{pk}(j) \neq m_1$ **or** $m_1 \leqslant 3m_2$,
12: Then remove this local extremum location;
13: **end if**
14: **end for**
15: **return** All remaining extremum locations.

Remarks. In step 11, the factor 3 is an empirical value obtained after trial and error with our algorithm to various databases. In situations where the sliding window does not contain a real QRS complex or where noise is retained in the reconstructed signal, we require a secondary test to assess whether the maximum point is significantly different from other local maximum points. For noisier datasets, factor 3 may lead to missed detections of QRS complex, and the value of this factor may be set at a smaller value.

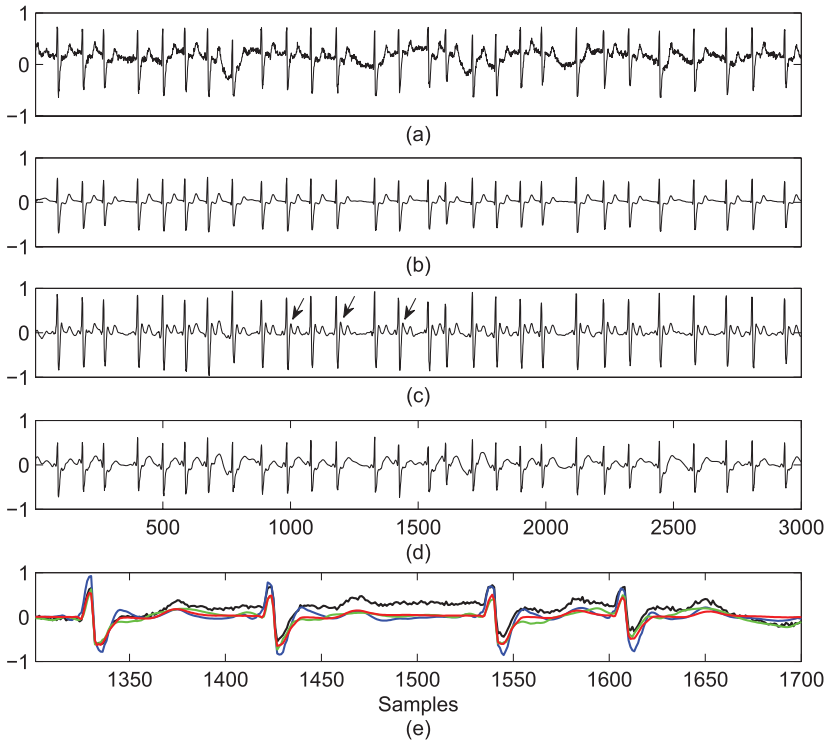

Figure 5. Denoised and baseline-corrected ECG recording s00262 in MIMIC II Matched Subset. (a) Input ECG recording with 3000 samples; (b)–(d) show the denoised and baseline-corrected ECG signals derived using our proposed algorithm 1, the EMD-ST algorithm and the DWT-T algorithm, respectively; (e) magnified details of the ECG waves derived from samples 1301 to 1700. The black, red, green, and blue lines denote the original ECG recording, and the results from our algorithm, the DWT-T algorithm and the EMD-ST algorithm, respectively. The arrows in (c) are pointing to the over-shock generated by the EMD-ST algorithm.

To evaluate our algorithm in more detail, we compare our algorithm with two other state-of-the-art ECG denoising algorithms, the EMD soft-thresholding algorithm (Blanco-Velasco *et al* 2008) (denoted by EMD-ST) and the wavelet thresholding algorithm (Abdelmounim *et al* 2014) (denoted by DWT-T), using another real-life ECG recording. As shown in figure 5(a), the input ECG waves differ from standard ECG waves. Figures 5(b)–(d) show the results derived using our algorithm and the EMD-ST and DWT-T approaches, respectively. Because the input signal does not contain strong noise, all tested algorithms perform well in terms of denoising and correction of the baseline. However, if we look closely at figure 5(c), we can find that, during each beat, between QRS-complex and T-wave, EMD-ST algorithm will generate a small over-shock, which is more evident by closer investigation of the plots in figure 5(e). This may arise from the asymmetry of this specific QRS complex, which departs from the IMF definition, where it is defined as the mono-component signal in the EMD algorithm. In figure 5(d), we can find that the DWT-T algorithm can also preserve the QRS-complex well, but it does not remove the baseline wandering completely.

Finally, we use a simulated ECG signal for quantitative comparison of the performance of our proposed algorithm with that of the other two algorithms. The clean ECG signal is the recording s00052 from the MIMIC II Matched Subset. We selected 10 clean segments from

Table 1. SNR improvement and root-mean-square error (RMSE) of simulated experiments.

	SNR_{imp}/RMSE		
Methods / Input (SNR/RMSE)	EMD threshold	DWT threshold	Proposed algorithm
10 dB/0.281	7.92/0.113	9.04/0.098	**13.45/ 0.059**
15 dB/0.193	9.17/0.067	11.13/0.052	**17.21/ 0.026**
20 dB/0.160	11.54/0.045	16.49/0.036	**21.22/ 0.013**

the signal, with each containing 2000 samples. For each segment, we subsequently added Gaussian white noise with various signal-to-noise ratio (SNR) values (generated using the MatLab function *awgn* with values of 10 dB, 15 dB and 20 dB) and a baseline wander (generated using $\cos(2\pi t)$). We then used different algorithms to remove the baseline wandering and the noise from each of the simulated signals. After that, we then compared the mean performances of these 10 signals based on two metrics: improvement in the SNR (denoted by SNR_{imp}) and the root-mean-square error (RMSE), which are defined as:

$$SNR_{imp} = 10\log_{10}\frac{\sum_{i=1}^{n}(y[i]-x[i])^2}{\sum_{i=1}^{n}(\hat{x}[i]-x[i])^2}, \tag{10}$$

$$RMSE = \sqrt{\frac{1}{n}\sum_{i=1}^{n}(\hat{x}[i]-x[i])^2}\,. \tag{11}$$

As shown in equations (10) and (11), a higher SNR_{imp} value and a lower RMSE value represent better results.

Table 1 presents a comparison of these two metrics when applying our proposed algorithm, the EMD-ST algorithm and the DWT-T algorithm to the same group of simulated ECG signals. The results show that our algorithm outperforms the other two algorithms. As an illustration, we show a sample simulated noisy signal (with SNR = 15 dB) in figure 6(a), while figure 6(b) shows the denoised and baseline corrected result derived using our proposed algorithm. In figures 6(c) and (d), detailed comparisons can be found among the real clean signal, our result and the results when using the EMD-ST and DWT-T algorithms. The details clearly show that our derived denoised signal resembles the original clean signal more closely than either of the signals derived using the other two algorithms.

5.2. QRS complex detection experiments[6]

After ECG signal enhancement, we can use the sparse representation coefficients and the modified atoms to perform the QRS complex detection. Figures 4(a), 5(a) and 6(a) show the QRS complex detection results for the three examples in the MIMIC II database that were derived by our proposed algorithm 2. Because our ECG enhancement algorithm can remove most of the noise and baseline wandering, the QRS complex detection in these examples is effective.

For further evaluation of the QRS complex detection performance of our algorithm, we use the MIT-BIH database (Goldberger *et al* 2000) to test our algorithm and the other QRS complex detection approaches. We compare the performances of the different approaches based on three metrics: sensitivity, precision, and detection error. These metrics are calculated using

[6] The source codes of algorithm 2 (QRS detection algorithm) can be downloaded from http://mda.ia.ac.cn/people/huxy/codes/SparseECG.rar.

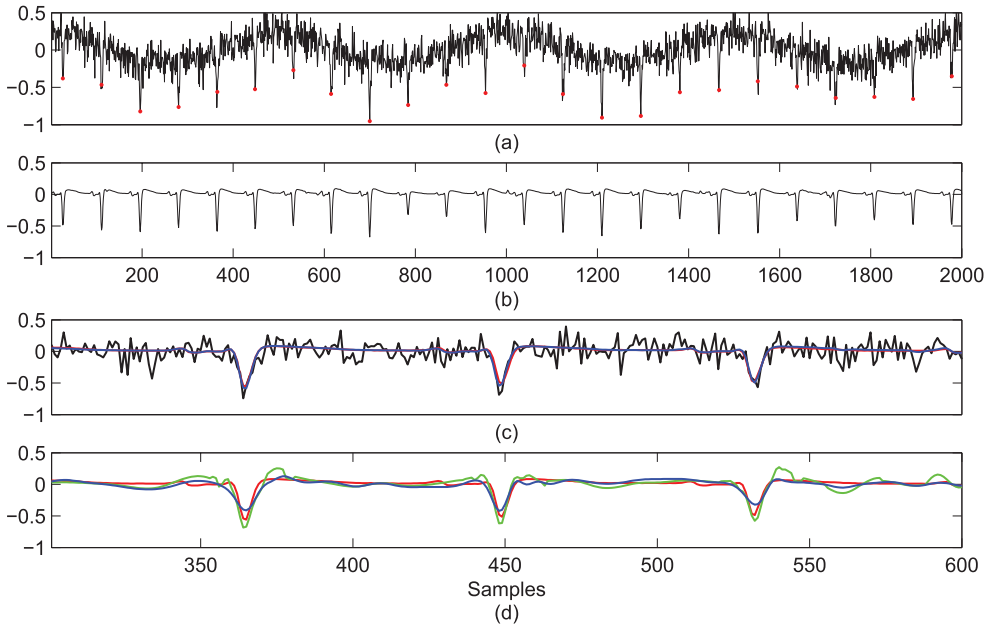

Figure 6. Simulated denoising and baseline correction experiment. (a) Simulated noisy and baseline wandering signal with a signal-to-noise ratio (SNR) =15 dB. (b) Denoised and baseline corrected signal derived using our algorithm. (c) Detailed comparison between noisy signal (black line), real clean signal (red line) and denoised signal derived using our approach (blue line). (d) Detailed comparison between real clean signal (red line), and the results of using EMD-ST (green line) and DWT-T (blue line).

$$\text{Sensitivity}(\%) = \frac{N_{\text{TP}}}{N_{\text{TP}} + N_{\text{FN}}}, \tag{12}$$

$$\text{Precision}(\%) = \frac{N_{\text{TP}}}{N_{\text{TP}} + N_{\text{FP}}}, \tag{13}$$

and

$$\text{Detection Error}(\%) = \frac{N_{\text{FN}} + N_{\text{FP}}}{N_{\text{TP}} + N_{\text{FN}}}, \tag{14}$$

respectively. In equations (12) to (14), N_{TP}, N_{FN}, and N_{FP} refer to the number of true positives, false negative prediction (i.e. the number of missing QRS complexes) and false positives (i.e. the number of falsely detected QRS complexes), respectively.

Table 2 shows the QRS complex detection results that were derived using our proposed algorithm 2 when applied to all 48 ECG data records in the MIT-BIH database. Because some of these records have very good signals and our algorithm can detect all the true QRS complexes correctly (both N_{FN} and N_{FP} equal to 0), we only show the records that have instances of either false negative or false positive detection in table 2. From this, we find that the detection rates for most records still show very high accuracy (with both sensitivity and precision rate being higher than 99%). Our algorithm does not perform well in only five records (records 105, 106, 108, 114, 207), in which the sensitivity or the precision rate are lower than 99%.

Table 2. Performance evaluation of proposed algorithm on MIT-BIH database.

Record	Total	N_{FN}	N_{FP}	Sensitivity (%)	Precision (%)	Error (%)
100	2272	0	1	100	99.96	0.04
101	1864	0	2	100	99.89	0.11
104	2228	0	11	100	99.51	0.49
105	2572	8	30	99.69	98.84	1.48
106	2027	39	0	98.08	100	1.92
107	2136	0	9	100	99.58	0.42
108	1762	32	16	98.18	99.08	2.72
109	2530	1	0	99.96	100	0.04
111	2122	1	0	99.95	100	0.05
114	1879	26	14	98.62	99.25	2.13
116	2410	2	4	99.92	99.83	0.25
119	1986	0	1	100	99.95	0.05
121	1861	1	0	99.95	100	0.05
200	2593	0	17	100	99.35	0.66
201	1943	11	1	99.43	99.95	0.62
202	2133	5	1	99.77	99.95	0.28
203	2980	6	0	99.79	100	0.20
205	2656	2	0	99.92	100	0.08
207	1886	43	1	97.72	99.95	2.33
208	2954	6	3	99.80	99.90	0.30
209	3004	0	2	100	99.93	0.07
210	2650	7	0	99.74	100	0.26
213	3248	0	4	100	99.88	0.12
214	2259	1	1	99.96	99.96	0.09
215	3362	5	0	99.85	100	0.15
217	2206	2	0	99.91	100	0.09
221	2427	0	9	100	99.63	0.37
222	2483	3	0	99.88	100	0.12
223	2604	1	0	99.96	100	0.04
228	2049	4	6	99.80	99.71	0.49
232	1780	7	5	99.61	99.72	0.67
234	2752	0	1	100	99.96	0.04

We then analyze our QRS detection performance more carefully using record 105 from the MIT-BIH database. Figure 7(a) shows the original ECG signal from 1316 to 1332 s, the reference QRS annotations (green circles) and the detected QRS complex (red dots) that were derived using our proposed algorithm 2. Figures 7(b) and (c) show the denoised and baseline-corrected ECG signals derived using our proposed algorithm 1 and the QRS peak information signal that was reconstructed using modified atoms, respectively. As shown in figures 7(b) and (c), our algorithm can remove the noise and the baseline wandering very well; also, the QRS peak information signal can correctly indicate the locations of all the QRS-like peaks. However, because our QRS detection algorithm does not use the normal RR-interval as the prior knowledge, it may lead to some false positive detection results (as seen near 1318 s).

The overall performance of our algorithm in the MIT-BIH database is shown in table 3, which also contains comparison results with other different approaches. The approaches used for comparison in table 3 include linear filtering (Zhu and Dong 2013), S-transform (Zidelmal *et al* 2014), Artificial neural network (Arbateni and Bennia 2014), Wavelet transform I (Bouaziz

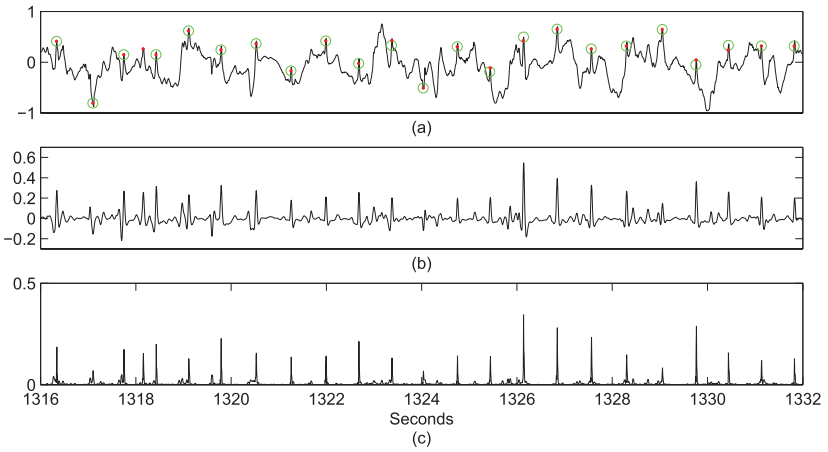

Figure 7. Denoised and QRS detected version of record 105 in MIT-BIH database. (a) Input ECG recording from 1316 to 1332 s; (b) denoised and baseline-corrected ECG signals derived using our proposed algorithm 1; (c) reconstructed QRS peak information signal. Note that in (a), the entire signal was normalized between −1 and 1, and the detected and reference annotations are marked using red dots and green circles, respectively.

Table 3. QRS detection performance comparison of proposed algorithm with other approaches using the MIT-BIH database.

Methods	N_{TP}	N_{FN}	N_{FP}	Sensitivity(%)	Precision(%)	Error(%)
Linear filtering	109 401	93	91	99.92	99.92	0.17
S-transform	108 323	171	97	99.84	99.91	0.25
Artificial neural network	109 273	210	109	99.81	99.91	0.28
Sparse representation	**109 224**	**213**	**139**	**99.81**	**99.87**	**0.32**
Wavelet transform I	109 354	140	232	99.87	99.79	0.34
Quadratic filtering	109 281	202	210	99.82	99.81	0.38
Mathematical morphology	109 297	213	204	99.80	99.81	0.38
Multiresolution entropy	109 692	273	163	99.75	99.85	0.39
Wavelet transform II	115 945	192	308	99.81	99.70	0.49
Wavelet transform III	109 118	376	218	99.66	99.80	0.54

et al 2014), Quadratic filtering (Phukpattaranont 2015), Mathematical morphology (Zhang and Lian 2009), Multiresolution entropy (Farashi 2016), Wavelet transform II (Karimipour and Homaeinezhad 2014), Wavelet transform III (Choi *et al* 2010), and our proposed algorithm (denoted as 'sparse representation'). Because the codes of these other approaches were not availabe, statistical data from Phukpattaranont (2015) were used. Because the other methods may have different QRS annotation references, the total number of QRS beats of the different

approaches may vary slightly. However, the average detection error rate can still reflect the general performance levels of the different algorithms, and thus we have ordered these methods based on this index in table 3. As shown in the table, for the MIT-BIH database, the performance of our proposed algorithm are comparable to other state-of-the-art approaches. Unlike some learning-based algorithms that can only train a model to detect QRS-complex, e.g. ANN-based algorithm (Arbateni and Bennia 2014), our algorithm can also enhance the ECG signals for further analysis and diagnosis. While for those fixed-basis based algorithms, like wavelet-based algorithms (Addison 2005), our proposed algorithm uses adaptive atoms to approximate the individual ECG signal. That means, our algorithm can extract the exact waveform morphology adaptively from a specific ECG lead signal and requires less subjective parameterizations. The adaptive learned dictionary can also be used for some further applications.

However, the learning-based algorithm do have some limitations. Compared with traditional derivative-based methods, a major drawback of learning-based approaches is that a sufficiently large training set must be set aside for training. This may present a problem for applications where only limited data is available. Another limitation of learning-based approaches is that the dictionary and coefficients learned from a subset of the ECG signal may not be always generalizable to the remainder of the signal when the signal is highly non-stationary. Therefore, building an abundant and diversified training dataset is an important issue for improving learning-based approaches.

Moreover, if an arrhythmia or abnormal ventricular conduction occurs infrequently in an ECG time series, there is risk that this algorithm will miss the different morphologies during the random selection process used to form a training set. In such cases, an anomaly detector proposed in Dunning and Friedman (2014) may be used to find whether the newly encountered morphology can be approximated by the current dictionary sparsely. If not, these morphologies may need to be added into the training set and updated into the dictionary to better enhance beat detection even in the presence of different rhythm types.

6. Conclusions

In this paper, a sparse representation-based ECG signal enhancement and QRS complex detection approach is presented. The sparse and redundant representation is a recently established signal analysis tool that can effectively learn inner structures from noisy input signals. First, we analyze the characteristics of the P-waves, T-waves, and QRS complexes in the ECG recordings and the smoothly-varying baseline wandering revealed in the learned dictionaries. Then, based on the characteristics of the atoms in the learned dictionary, we divide the dictionary into two subsets, and then extract the intrinsic ECG waves without the baseline wandering from the input ECG recording. Finally, the atoms with large kurtosis values have been modified to produce an impulse function that is used to locate the QRS complexes. The simulated and real-life experimental results demonstrate that our approach can effectively enhance ECG recordings with high noise levels and baseline wandering, and can then detect the QRS complexes correctly and accurately from these enhanced ECG signals.

Importantly, with the emergence of portable devices and need for real-time processing, our algorithm can easily be capable of real-time ECG signal enhancement and beat detection since the ECG reconstruction process using a sparse representation approach is not computationally heavy. The rate-limiting step is the actual training of the dictionary. To overcome this, certain steps can be taken to enhance efficiency. For instance, a subject's historic data can be used to construct a preliminary training set. If the ECG morphology changes due to variations in electrophysiology or electrode placement, then the new ECG morphology can be added into the

training set to update the dictionary. Because our training algorithm uses 'update and reuse' strategy (Smith and Elad 2013), the updating process of an already trained dictionary is also very fast. However, given the possible non-stationarities observed in an individual ECG, the frequency and overall effectiveness of these update remains largely unknown. So, the general implementation of this algorithm to such real-time systems and to clinical situations (with varying pathologies) warrants further study.

Acknowledgment

This work was partially supported by the National Natural Science Foundation of China with Grant No.61571438. Dr Ahn was supported by The Institute for Integrative Health. The authors also would like to thank the reviewers for their insightful comments, which helped improve the quality of the paper significantly.

References

Abdelmounim E, Haddadi R and Belaguid A 2014 Electrocardiogram signal denoising using discrete wavelet transform *Proc. IEEE Int. Conf. on Multimedia Computing and Systems* (IEEE) pp 1065–70

Addison P S 2005 Wavelet transforms and the ECG: a review *Physiol. Meas.* **26** R155

Aharon M, Elad M and Bruckstein A 2006 K-SVD: an algorithm for designing overcomplete dictionaries for sparse representation *IEEE Trans. Signal Proc.* **54** 4311–22

Akhbari M, Shamsollahi M B, Jutten C, Armoundas A A and Sayadi O 2016 ECG denoising and fiducial point extraction using an extended Kalman filtering framework with linear and nonlinear phase observations *Physiol. Meas.* **37** 203–66

Arbateni K and Bennia A 2014 Sigmoidal radial basis function ANN for QRS complex detection *Neurocomputing* **145** 438–50

Arzeno N M, Deng Z-D and Poon C-S 2008 Analysis of first-derivative based QRS detection algorithms *IEEE Trans. Biomed. Eng.* **55** 487–93

Blanco-Velasco M, Weng B and Barner K E 2008 Ecg signal denoising and baseline wander correction based on the empirical mode decomposition *Comput. Biol. Med.* **38** 1–13

Bouaziz F, Boutana D and Benidir M 2014 Multiresolution wavelet-based QRS complex detection algorithm suited to several abnormal morphologies *IET Signal Proc.* **8** 774–82

Chan H-L, Chen G-U and Lin M-A 2006 Heartbeat detection using energy thresholding and template match *Proc. 27th Annual Int. Conf. of the Engineering in Medicine and Biology Society* (IEEE) pp 6668–70

Choi S, Adnane M, Lee G-J, Jang H, Jiang Z and Park H-K 2010 Development of ECG beat segmentation method by combining lowpass filter and irregular R-R interval checkup strategy *Expert Syst. Appl.* **37** 5208–18

Dobbs S E, Schmitt N M and Ozemek H S 1984 QRS detection by template matching using real-time correlation on a microcomputer *J. Clin. Eng.* **9** 197–212

Dunning T and Friedman E 2014 *Practical Machine Learning: a New Look at Anomaly Detection* 1st edn (Sebastopol, CA: O'Reilly Media)

Engan K, Skretting K and Husøy J H 2007 Family of iterative ls-based dictionary learning algorithms, ils-dla, for sparse signal representation *Digit. Signal Process.* **17** 32–49

Farashi S 2016 A multiresolution time-dependent entropy method for QRS complex detection *Biomed. Signal Process. Control* **24** 63–71

Goldberger A L, Amaral L A, Glass L, Hausdorff J M, Ivanov P C, Mark R G, Mietus J E, Moody G B, Peng C-K and Stanley H E 2000 PhysioBank, PhysioToolkit, and PhysioNet: components of a new research resource for complex physiologic signals *Circulation* **101** e215–20

Hu X, Peng S and Hwang W-L 2012 EMD revisited: a new understanding of the envelope and resolving the mode-mixing problems in AM-FM signals *IEEE Trans. Signal Process.* **60** 1075–86

Johnson A E W, Behar J, Andreotti F, Clifford G D and Oster J 2015 Multimodal heart beat detection using signal quality indices *Physiol. Meas.* **36** 1665–79

Kabir M A and Shahnaz C 2012 Denoising of ecg signals based on noise reduction algorithms in emd and wavelet domains *Biomed. Signal Process. Control* **7** 481–9

Karimipour A and Homaeinezhad M R 2014 Real-time electrocardiogram P-QRST detection-delineation algorithm based on quality-supported analysis of characteristic templates *Comput. Biol. Med.* **52** 153–65

Mailhé B, Lesage S, Gribonval R and Bimbot F 2008 Shift-invariant dictionary learning for sparse representations: extending K-SVD *Proc. European Signal Processing Conf.* pp 1–4

Ning X and Selesnick I W 2013 ECG enhancement and QRS detection based on sparse derivatives *Biomed. Signal Process. Control* **8** 713–23

Pal S and Mitra M 2012 Empirical mode decomposition based ECG enhancement and QRS detection *Comput. Biol. Med.* **42** 83–92

Pati Y C, Rezaiifar R and Krishnaprasad P 1993 Orthogonal matching pursuit: recursive function approximation with applications to wavelet decomposition *Proc. 27th Asilomar Conf. on Signals, Systems and Computers* (IEEE) pp 40–4

Phukpattaranont P 2015 QRS detection algorithm based on the quadratic filter *Expert Syst. Appl.* **42** 4867–77

Smith L N and Elad M 2013 Improving dictionary learning: multiple dictionary updates and coefficient reuse *IEEE Signal Process. Lett.* **20** 79–82

Tosic I and Frossard P 2011 Dictionary learning *IEEE Signal Process. Mag.* **28** 27–38

Tracey B H and Miller E L 2012 Nonlocal means denoising of ecg signals *IEEE Trans. Biomed. Eng.* **59** 2383–6

Yi X, Hu X and Peng S 2013 An operator-based and sparsity-based approach to adaptive signal separation *Proc. IEEE Int. Conf. on Acoustics, Speech and Signal Processing* (IEEE) pp 6186–90

Zhang F and Lian Y 2009 QRS detection based on multiscale mathematical morphology for wearable ECG devices in body area networks *IEEE Trans. Biomed. Circuits Syst.* **3** 220–8

Zhou Y, Hu X, Tang Z and Ahn A C 2015 Denoising and baseline correction of ECG signals using sparse representation *Proc. IEEE Workshop on Signal Process Systems* (IEEE) pp 1–6

Zhu H and Dong J 2013 An R-peak detection method based on peaks of shannon energy envelop *Biomed. Signal Process. Control* **8** 466–74

Zidelmal Z, Amirou A, Adnane M and Belouchrani A 2012 QRS detection based on wavelet coefficients *Comput. Methods Programs Biomed.* **107** 490–6

Zidelmal Z, Amirou A, Ould-Abdeslam D, Moukadem A and Dieterlen A 2014 QRS detection using S-Transform and Shannon energy *Comput. Methods Programs Biomed.* **116** 1–9